

Supplementary Materials

Percolation-induced resistivity drop in lutetium dihydride with controllable electrical conductivity over six orders of magnitude

Ningning Wang^{1,2#*}, Jun Hou^{1,2#}, Ziyi Liu^{1,2}, Tenglong Lu^{1,2}, Pengfei Shan^{1,2}, Congcong Chai^{1,2}, Shifeng Jin^{1,2}, Liang Ma^{1,3,4}, Lifan Shi^{1,2}, Xiao Wang^{1,2}, Youwen Long^{1,2,5}, Yue Liu^{1,2}, Hua Zhang^{1,2}, Xiaoli Dong^{1,2}, Sheng Meng^{1,2,3}, Miao Liu^{1,5,6*} and Jinguang Cheng^{1,2*}

¹Beijing National Laboratory for Condensed Matter Physics and Institute of Physics, Chinese Academy of Sciences, Beijing 100190, China

²School of Physical Sciences, University of Chinese Academy of Sciences, Beijing 100190, China

³Key Laboratory of Materials Physics, Ministry of Education, School of Physics and Microelectronics, Zhengzhou University, Zhengzhou 450052, China

⁴Institute of Quantum Materials and Physics, Henan Academy of Sciences, Zhengzhou 450046, China

⁵Songshan Lake Materials Laboratory, Dongguan, Guangdong 523808, China

⁶Center of Materials Science and Optoelectronics Engineering, University of Chinese Academy of Sciences, Beijing 100049, China

These authors contributed equally to this work.

*Corresponding authors: nnwang@iphy.ac.cn; mliu@iphy.ac.cn; jgcheng@iphy.ac.cn

Sample preparation

Because the hydrogenation process is usually employed to convert ductile rare-earth metals to brittle hydrides in order to facilitate the pulverization process, the main phase of most commercially purchased “rare-earth” powders are actually rare-earth dihydrides. In the present study, we used the commercially available “Lu” powder (99.9%, JiangXi Viilaa Metal Material Co., Ltd.) as the starting material. Rietveld refinements on the powder XRD pattern confirmed that the major phase is the cubic LuH₂ (95%) coexisting with minor Lu (5%) and some unidentified phases, as shown in Fig. S1. Thus, the as-received “Lu” powder is dark blue in color and contains mainly the LuH₂ grains with different sizes ranging from ~200 μm to submicron. The dense pellets of LuH₂ were prepared by cold pressing at 4 GPa using a large-volume press.

Physical properties measurement.

The resistivity and heat capacity were measured with a Physical Property Measurement System, while the magnetic properties were measured with a Magnetic Property Measurement System from Quantum Design. During the resistivity measurements from 2-300 K, we used a sweep rate of 2 K/min to avoid the thermal hysteresis behavior due to the difference between the instrument thermometer and the actual temperature of the sample in the cooling-down and warming-up processes.

X-ray characterization.

Low-temperature XRD data in the temperature range 100-300 K were collected on a Rigaku Smartlab diffractometer with Cu-K α radiation equipped with a low-temperature chamber providing variable temperature within 5-300 K.

Calculations

The structural optimization, phonon dispersions, electron-phonon coupling (EPC), and superconducting properties were carried out under 0 and 10 GPa with the QUANTUM ESPRESSO (QE) package. The plane-wave kinetic-energy cutoff and the energy cutoff for charge density were set as 100 and 400 Ry, respectively. A Methfessel-Paxton smearing width of 0.02 Ry was adopted to calculate the self-consistent electron density. A Brillouin zone (BZ) k-point mesh of $12 \times 12 \times 12$ was adopted for LuH₂ and LuN, and a $6 \times 6 \times 6$ BZ k-point mesh was chosen for LuH₃ instead. The dynamic and EPC matrix elements were computed with an $8 \times 8 \times 8$ q mesh. The density functional perturbation (DFPT) and Eliashberg theories were used to quantify the phonon and EPC properties.

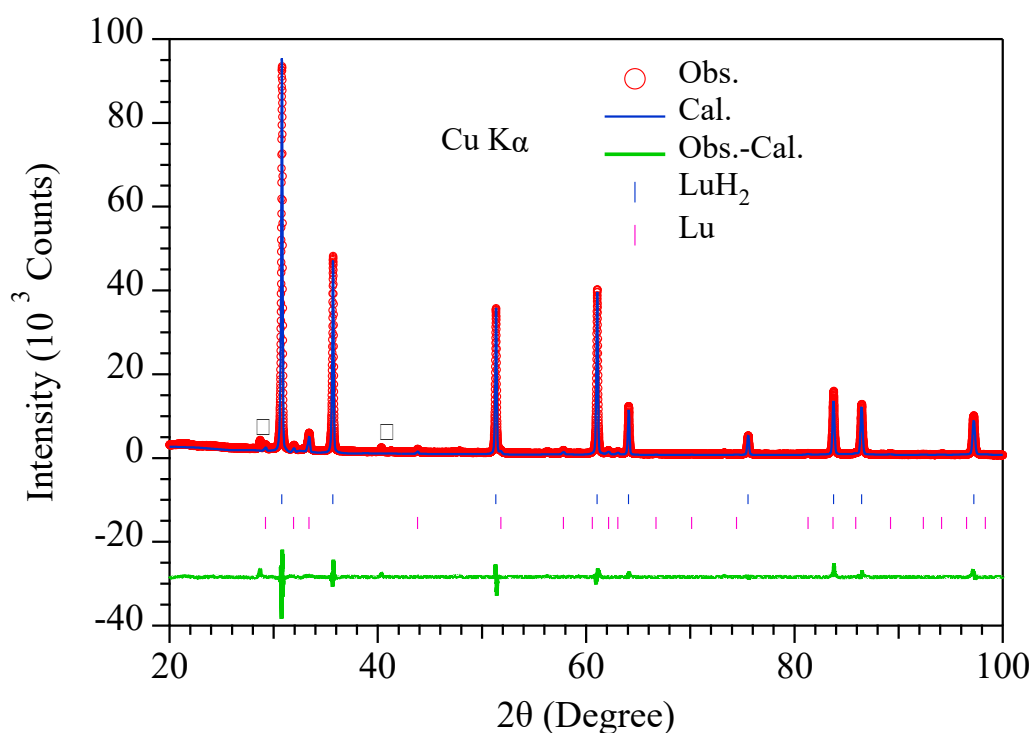


Figure S1. Observed (circle), calculated (solid line), and difference (bottom line) XRD profiles of the commercially purchased “Lu” powder measured at room temperature after Rietveld refinements. The Bragg positions are shown as the tick marks. Two additional weak peaks at 28.70° and 40.35° marked by asterisks come from some unknown phases, which thus cannot be considered in the Rietveld refinement.

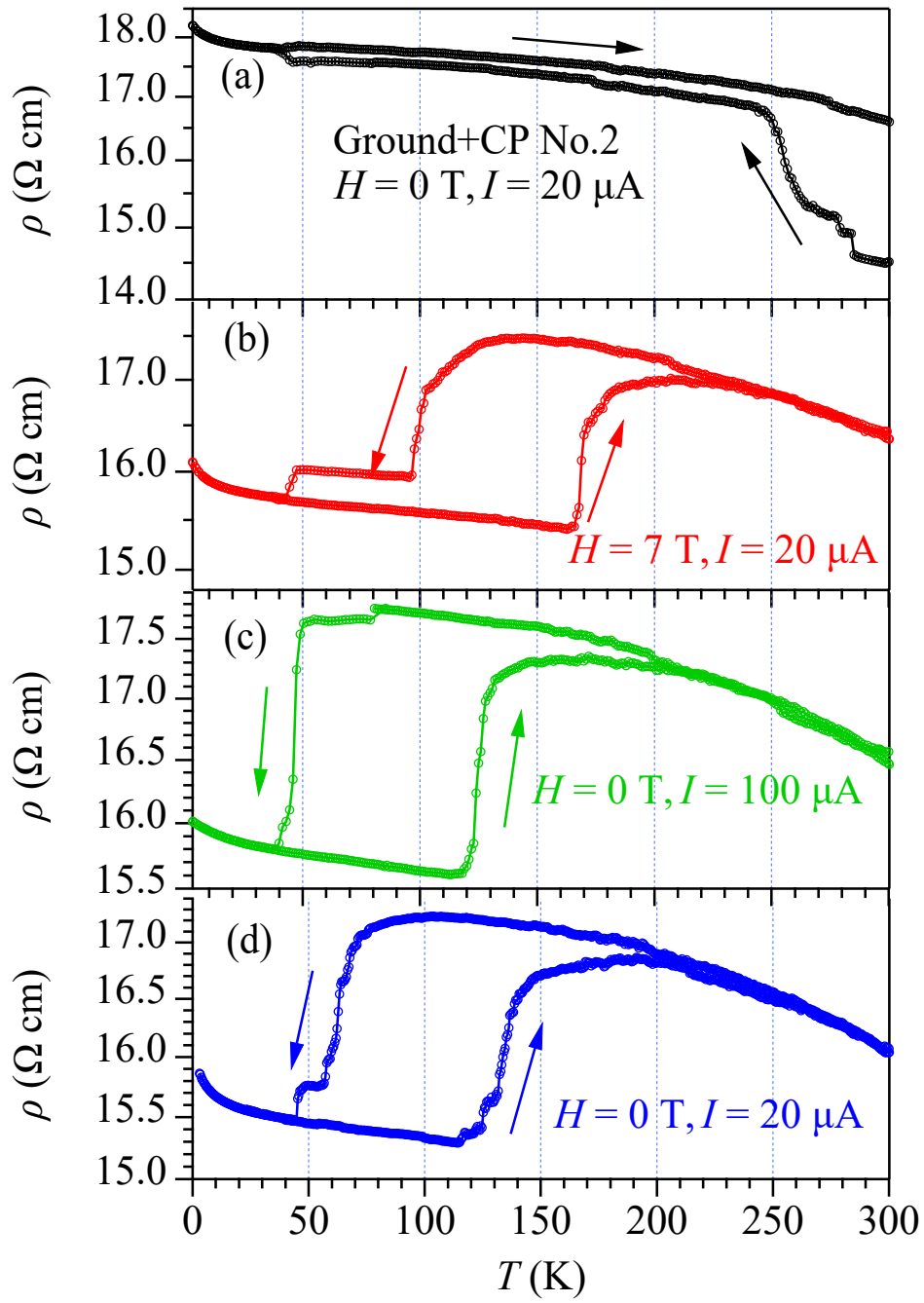


Figure S2. Temperature-dependent resistivity $\rho(T)$ of another “Ground+CP” LuH_2 showing a drop/jump behavior. The arrows indicate the cooling-down and warming-up processes.

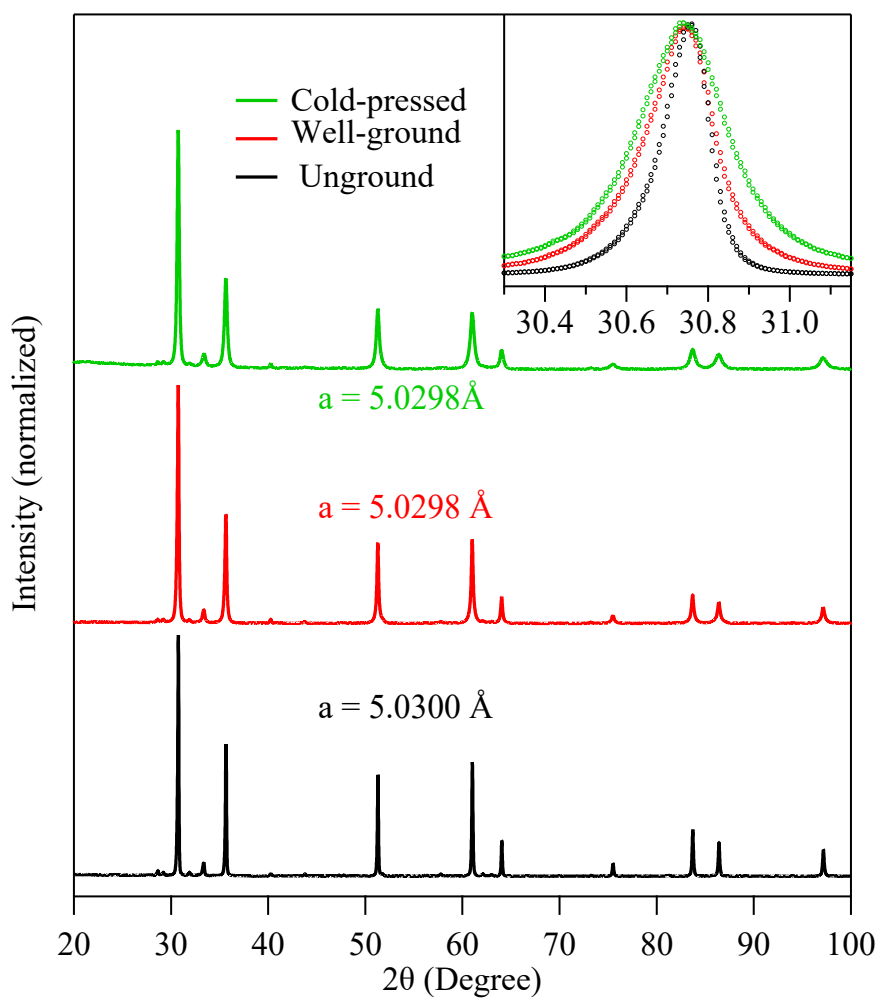


Figure S3. Powder XRD patterns of three kinds of LuH₂ samples with different treatments: as-received powder (bottom), ground powder (middle), and powder of CP sample (top). The inset shows the main peak of these LuH₂ samples.

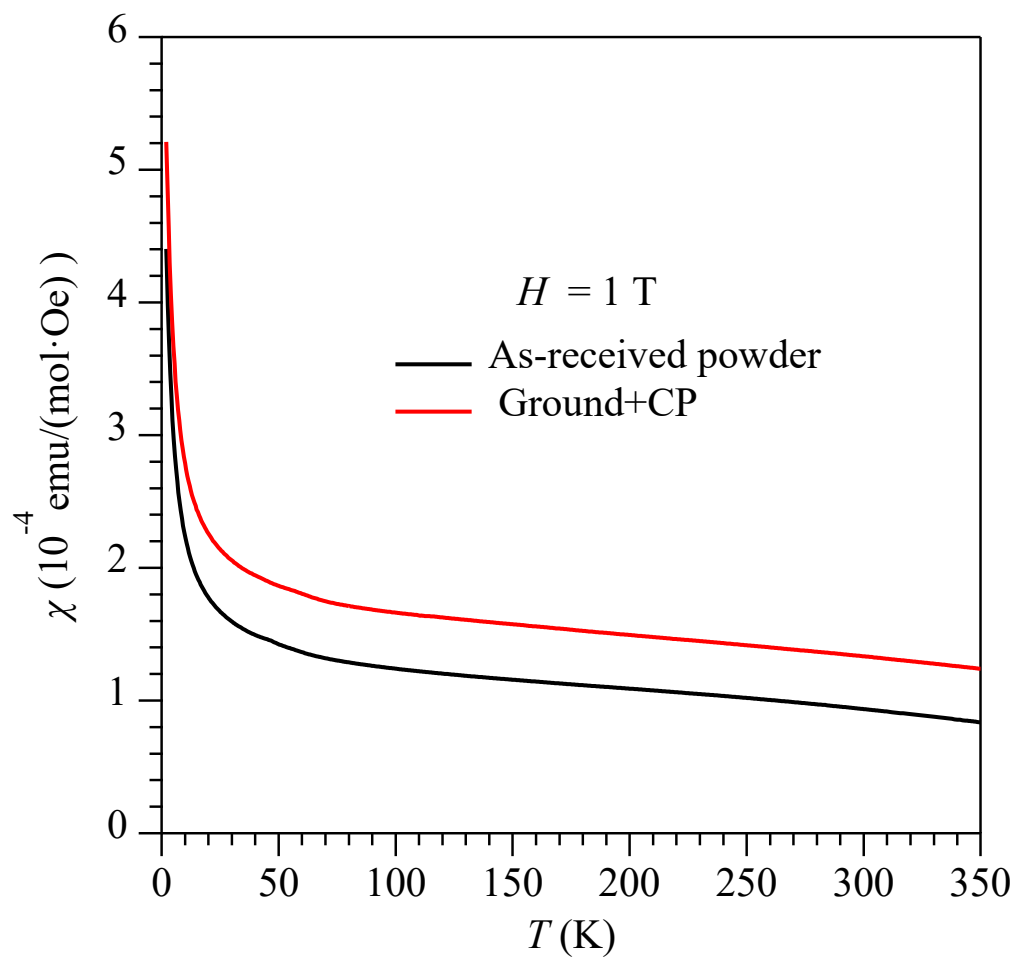


Figure S4. Temperature-dependent dc magnetic susceptibility $\chi(T)$ of the as-received powder and the “Ground+CP” samples of LuH₂.

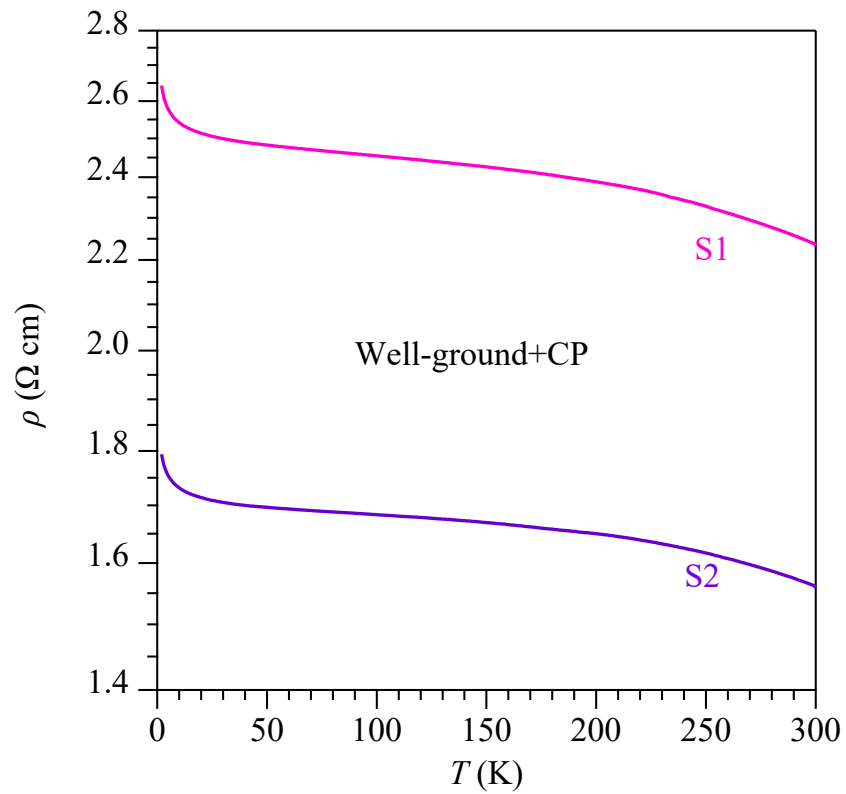


Figure S5. Temperature-dependent resistivity $\rho(T)$ of the CP LuH₂ sample made of as-received powders after grinding for 30 minutes.

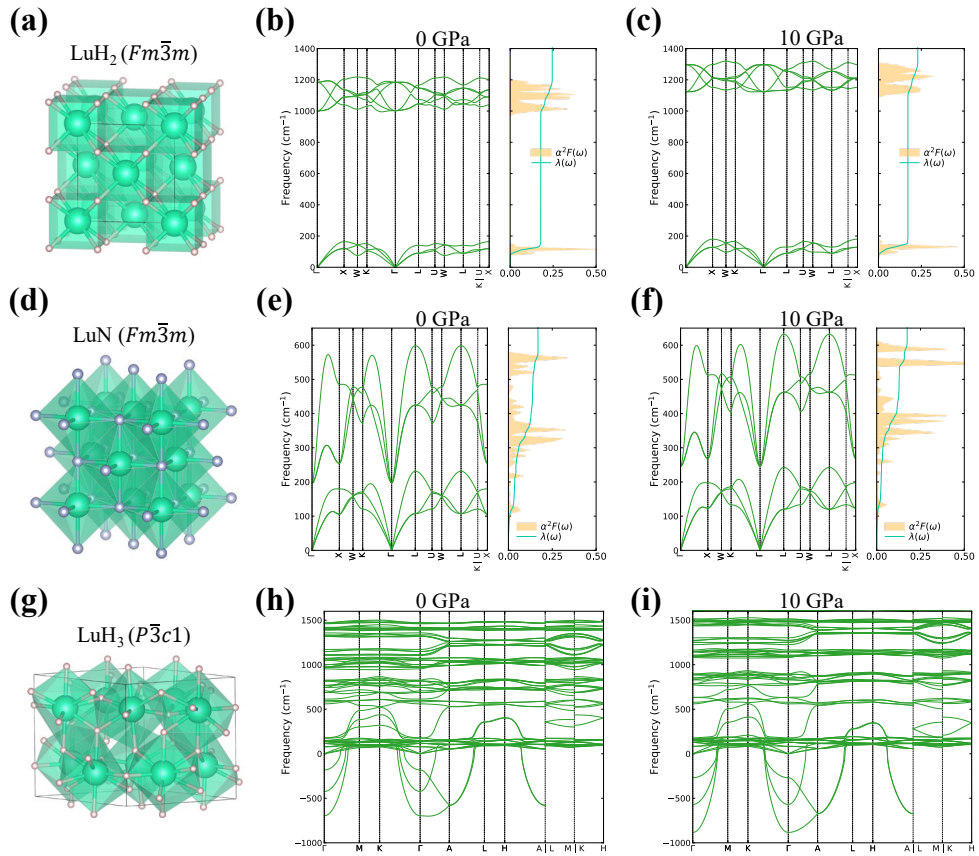


Figure S6. Calculated electron-phonon interactions of (b) LuH₂ at 0 GPa, (c) LuH₂ at 10 GPa, (e) LuN at 0 GPa, (f) LuN at 10 GPa, (h) LuH₃ at 0 GPa, and (i) LuH₃ at 10 GPa. Detailed crystal structures of (a) LuH₂, (d) LuN, and (g) LuH₃ were shown in left panels.

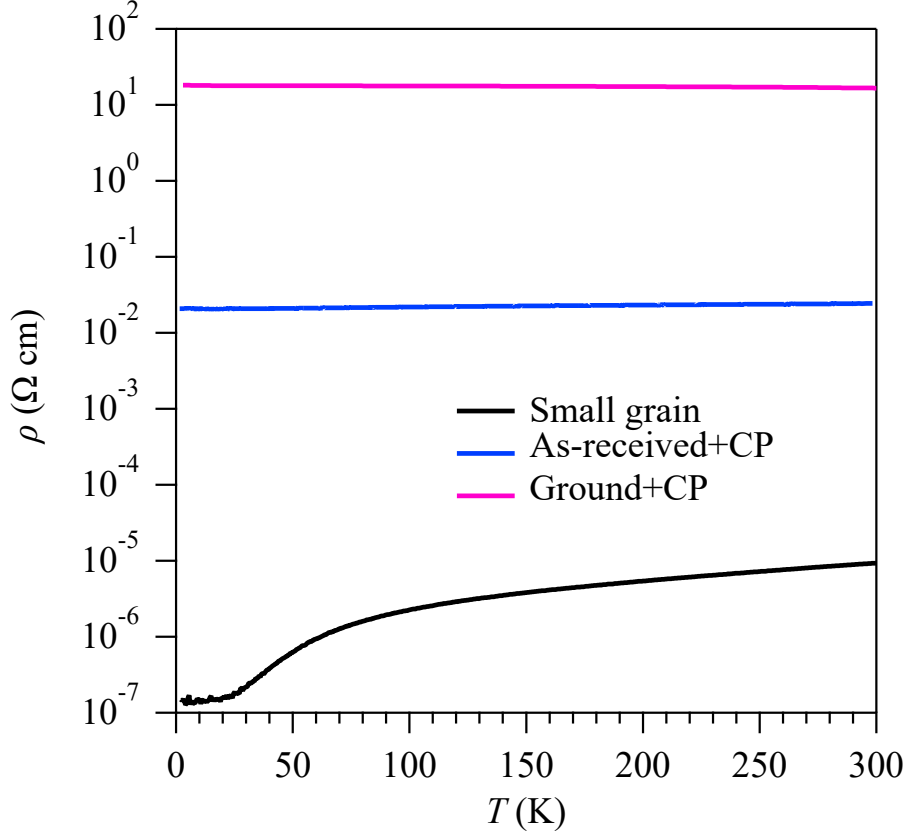


Figure S7. Temperature-dependent resistivity $\rho(T)$ of LuH₂ samples with different treatments: the small grain (bottom), “As-received+CP” (middle), and “Ground+CP” sample (top).

Table S1. The electron phonon coupling constant λ , logarithmic average frequency ω_{ln} , and superconducting critical temperature T_c for LuH₂, LuN, and LuH₃ under 0 and 10 GPa. For LuH₃, despite its thermodynamic stability, we predicted it was dynamically unstable under 0 and 10 GPa. Hence, we did not calculate its superconducting properties.

Formula	IDs		Pressure (GPa)	λ	ω_{ln} (K)	T_c (K)	Is superconductor
	Atomly	ICSD					
LuH ₂	1000314722	56067	0	0.259	300	0.026	Yes
			10	0.242	315	0.010	Yes
LuN	3001350567	44779	0	0.179	410	0.000	No
			10	0.167	497	0.000	No
LuH ₃	0000079762	638277	0	–	–	–	–
			10	–	–	–	–